PHILOSOPHICAL TRANSACTIONS OF THE ROYAL SOCIETY A MATHEMATICAL, PHYSICAL & ENGINEERING SCIENCES

A Magnetic Model of the Solar Transition Region

A. H. Gabriel

Phil. Trans. R. Soc. Lond. A 1976 **281**, 339-352
doi: 10.1098/rsta.1976.0031

Phil. Trans. R. Soc. Lond. A. **281**, 339–352 (1976) [339]
Printed in Great Britain

A magnetic model of the solar transition region

By A. H. Gabriel
Appleton Laboratory Astrophysics Research Division, Culham Laboratory, Abingdon, Oxon

A two-dimensional model of the chromosphere and corona has been constructed. This is based upon the magnetic flux concentrations which occur at the boundaries of the supergranule convection cells. The expansion of the magnetic flux is determined by the vertical extent of the convecting plasma. The distribution of atmospheric material is consistent both with observed spectral intensities and with energy balance requirements. The model predicts a primary transition region which is confined to an area about 10″ wide overlying the supergranule boundaries. A secondary transition region which is much thinner covers the cell centres. The predictions are fully consistent with recent ultraviolet observations.

1. Introduction

It is well known that models of the solar atmosphere based upon spherical symmetry or plane parallel theories can only be an approximation. However, the real question concerns how meaningful such approximations can be. It is possible, for certain applications, to define a mean atmospheric model giving average values of the various physical parameters as a function of height. The averaging involved is subject to weighting factors, which vary with the type of observation, and the direction of viewing. It is, therefore, not surprising that there are differences between models obtained by different methods, and uncertainties concerning which model to apply in a given situation.

So long as inhomogeneities are completely random, their treatment is very complex. However, recent ultraviolet observations have shown that the principal departure from symmetry in quiet areas of the Sun is due to a very regular form of inhomogeneity; the influence of the supergranule convection cell. These cells cover the entire solar surface. They have a constant diameter of *ca.* 30 000 km and lead to a regular pattern of intensities and magnetic fields. Since the modulation of intensities can be as high as 10 : 1 it is clearly of importance to take account of this effect.

Attempts have been made in the past to investigate some of these effects (Kopp & Kuperus 1968; Kopp 1972). These have been somewhat limited in scope, and have led to some misleading predictions. The present paper attempts to derive a model based upon a more realistic description of the magnetic field geometry (the primary cause of the effect). A preliminary note on this work has been published previously (Gabriel 1974).

In the following sections we show first the discrepancies that arise when a spherically symmetric solar model is derived from two different approaches. A two-dimensional model is then constructed, based upon the supergranule network. It is shown that with this geometry, the discrepancies between the two approaches become much smaller and a self-consistent model can be produced. The predictions from this model are compared with a number of different types of observation and found to be broadly consistent.

2. Spherically symmetric analysis

We consider two methods of approach for the determination of a mean spherically symmetric solar atmosphere. The first involves the analysis of the observed absolute intensities of a number of optically thin emission lines; the second is based upon analysis of energy balance in the solar atmosphere.

2.1. *Analysis of absolute intensities*

This method has been used widely by a number of workers (e.g. Jordan 1965; Athay 1966; Dupree & Goldberg 1967) to derive spherical models from the observed intensities of optically thin lines. Each spectral line is used to derive a value of emission measure, $\langle N_e^2 \mathrm{d}h/\mathrm{d}\lg T\rangle$, at an effective temperature at which the emission function for that line

$$g(T) = (N_1/N_E)\, T^{-\frac{1}{2}} \exp -(E/kT) \tag{1}$$

would be a maximum. N_e, N_1 and N_E are the electron, ion and element densities, T is the electron temperature and E is the excitation potential. With a large number of lines, a curve for the variation of $\langle N_e^2 \mathrm{d}h/\mathrm{d}\lg T\rangle$ with T can be obtained. This can be integrated, providing some additional assumption is made, e.g. that of hydrostatic equilibrium:

$$\mathrm{d}p/p = \rho g\, \mathrm{d}h \tag{2}$$

where p is the pressure, ρ the density and g the gravitational acceleration. For a further discussion of this approach the reader is referred to Jordan & Wilson (1971).

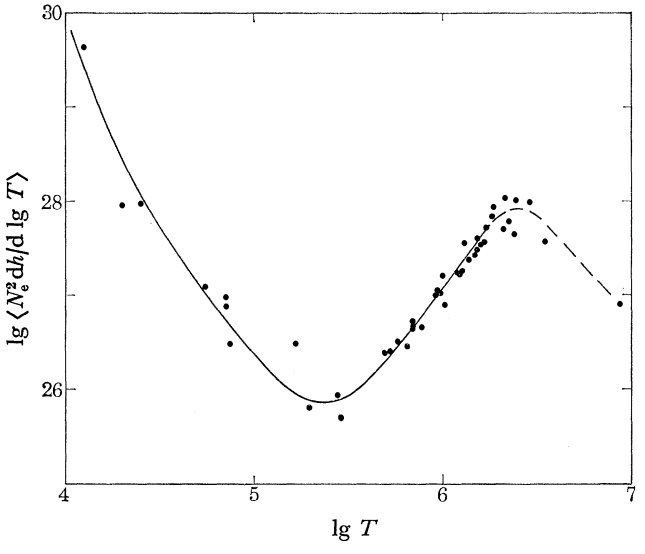

Figure 1. Emission measure derived from absolute intensities of observed spectra.

This method has now been applied to two sets of recent data. The first is an observation in the grazing-incidence by Malinovsky & Heroux (1973). The second is a normal-incidence observation from the OSO-6 satellite by Dupree *et al.* (1973). They have both been re-analysed using recent atomic data, and the resulting emission measure curve is shown in figure 1. The portion of the curve above lg T of 6.2 has been shown dashed, since the contribution from small active regions is known to dominate at these high temperatures. The effect of integrating this in conjunction with equation (2) leads to the structure as a function of height, shown as model A in figure 2.

Table 1 gives the essential parameters of the derived model. The boundary condition density in the corona has been selected to fit with other coronal observations. The height scale is above an arbitrary zero.

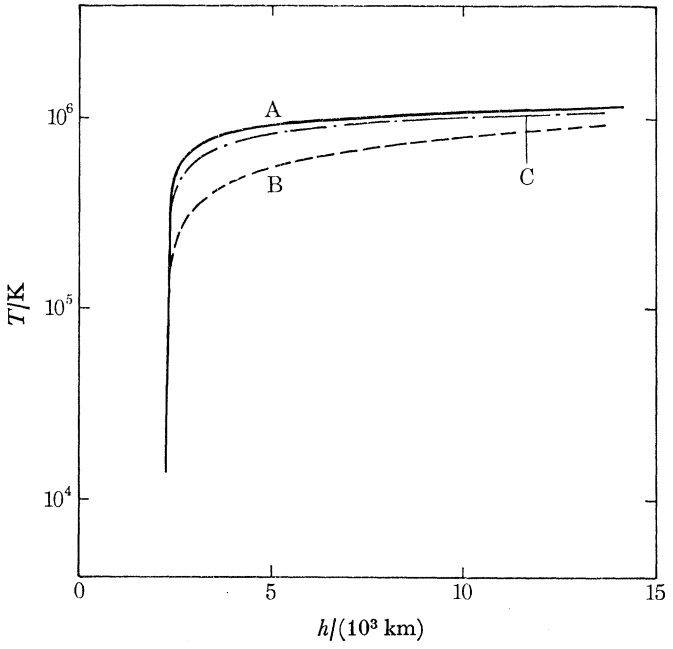

FIGURE 2. Temperature structure derived from (A) spherical model based on observed intensities in figure 1, (B) spherical model based on energy balance and (C) network model based on energy balance for regions overlaying s.g.b. The zero of height is arbitrary.

TABLE 1

	spherical absolute intensity model (model A)			network absolute intensity model (at s.g.b.) (model D)		
lg T	$\frac{H}{\text{km}}$	lg $\left\{\frac{N}{\text{cm}^{-3}}\right\}$	lg $\left\{\frac{-F_c}{\text{erg}\dagger\ \text{cm}^{-2}\ \text{s}^{-1}}\right\}$	$\frac{H}{\text{km}}$	lg $\left\{\frac{N}{\text{cm}^{-3}}\right\}$	lg $\left\{\frac{-F_c}{\text{erg cm}^{-2}\ \text{s}^{-1}}\right\}$ (local value)
4.3	1645	10.45	2.26	3322	10.57	1.75
4.4	1659	10.34	2.81	3384	10.45	2.24
4.5	1670	10.24	3.31	3429	10.33	2.70
4.6	1677	10.14	3.77	3464	10.22	3.13
4.7	1683	10.04	4.18	3493	10.11	3.54
4.8	1688	9.94	4.59	3518	10.01	3.94
4.9	1692	9.84	4.98	3539	9.91	4.41
5.0	1696	9.73	5.35	3558	9.81	4.75
5.1	1700	9.63	5.69	3576	9.71	5.10
5.2	1705	9.53	6.02	3595	9.60	5.40
5.3	1710	9.43	6.28	3617	9.50	5.63
5.4	1716	9.33	6.45	3648	9.40	5.79
5.5	1727	9.23	6.54	3702	9.30	5.86
5.6	1755	9.13	6.47	3807	9.20	5.87
5.7	1842	9.03	6.29	4057	9.09	5.83
5.8	2140	8.93	6.11	4731	8.98	5.77
5.9	3081	8.82	5.97	6403	8.86	5.74
6.0	6122	8.69	5.81	10450	8.73	5.71
6.1	16190	8.51	5.53	26360	8.51	5.50
6.15	32540	8.37	5.24	37850	8.37	5.30

† 1 erg = 10^{-7} J.

2.2. *Energy balance models*

The divergence of the conductive flux, F_c, can be expressed in terms of the difference between radiative losses R and a term representing the local dissipation of mechanical energy, S.

$$-\nabla \cdot \boldsymbol{F}_c = R - S \tag{3}$$

where $\nabla \cdot \boldsymbol{F}_c = \mathrm{d}F_c/\mathrm{d}h$ for spherical symmetry.

$$F_c = -cT^{\frac{5}{2}}\mathrm{d}T/\mathrm{d}h, \tag{4}$$

$$R = \eta(T)\, N_e^2, \tag{5}$$

and $$c = 1.23 \times 10^{-6}\,\mathrm{erg\ cm^{-1}\ s^{-1}\ K^{-\frac{7}{2}}}$$

the coefficient of thermal conduction appropriate for coronal plasma. This can be integrated, providing we again assume the equation of hydrostatic equilibrium (equation (2)), and make some assumption about S. Models can be derived on the assumption that $S = 0$, or that all the mechanical energy is deposited at a greater height than is being considered. Such models have been calculated by McWhirter *et al.* (1975). One such model is shown as model B in figure 2. Again the absolute height scale is arbitrary and has been adjusted to coincide for the two models in the transition region.

2.3. *Intercomparisons*

Comparison of models A and B of figure 2 show that there is a significant difference between them, the energy balance model not reaching 10^6 K until a much greater height than the absolute intensity model. There are other ways of making this comparison in which the discrepancy is more convincing.

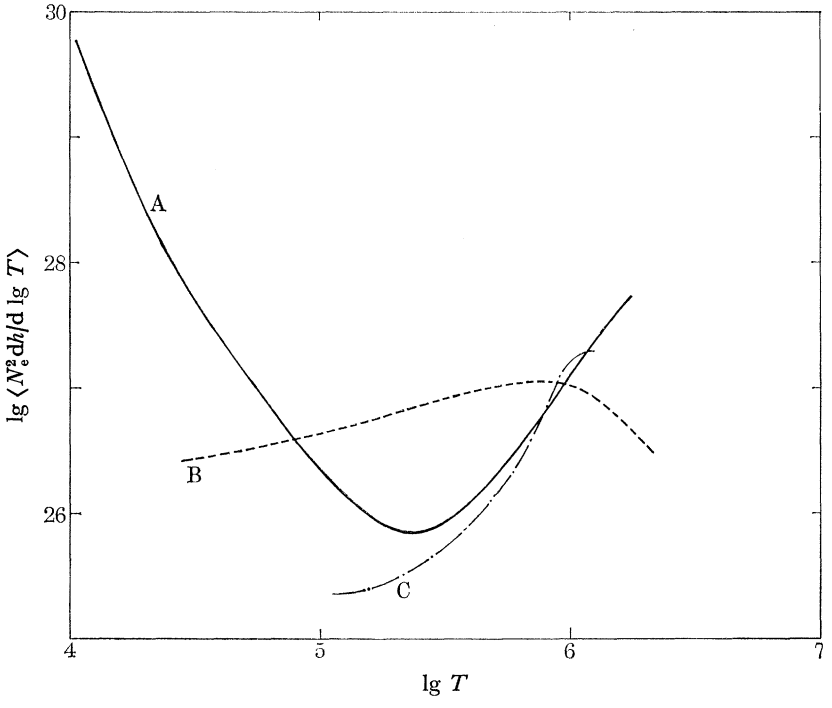

FIGURE 3. Curves of emission measure: (A) observed as in figure 1, (B) spherical energy balance model and (C) network energy balance model.

It is possible to compute for the energy balance model the predicted intensities of line emission, which can then be compared with observations. An equivalent and more convenient approach is to compute the emission measure $\langle N_e^2 \, \mathrm{d}h/\mathrm{d} \lg T \rangle$, which can be compared with emission measures derived from observations. This is shown in figure 3 where the curve from observed spectra (as plotted in figure 1) has been reproduced as curve A together with curve B derived from the energy balance model. A large discrepancy is seen.

An alternative approach is to examine the structure obtained from the absolute intensities, to see how far it is consistent with energy balance requirements. Using the derived structure and equation (4), it is possible to compute $\nabla \cdot F_c$. By using the radiation loss R per unit volume derived from equation (5), it is then possible by using equation (3) to derive the mechanical energy deposition S. This is shown as curve A in figure 4. For the energy balance model B, the value of S would of course be zero. Figure 4 shows S to depart substantially from zero, and the energy deposited or lost from the plasma per unit area can be obtained by integrating the shaded areas.

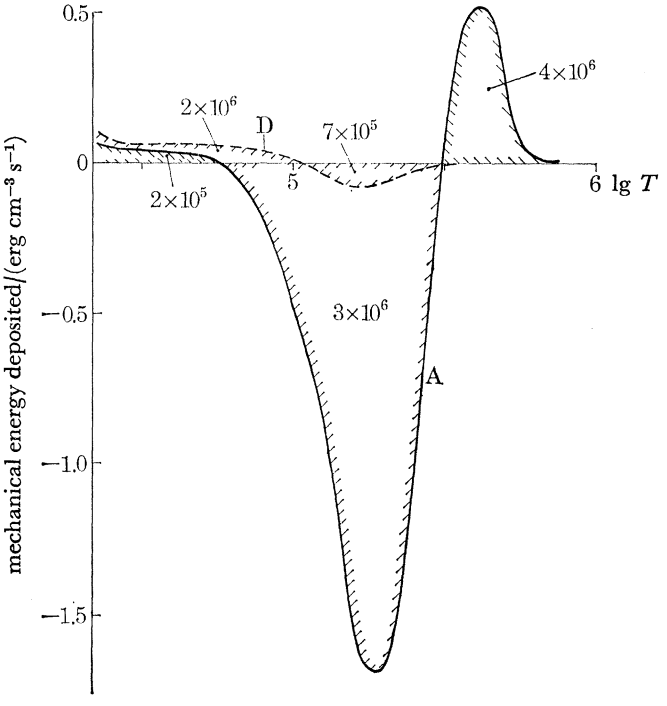

FIGURE 4. Mechanical energy deposit required by models based upon observed intensities: (A) spherical model, (D) network model. The figures within the shaded areas (erg $\mathrm{cm}^{-2}\,\mathrm{s}^{-1}$) represent the integrated requirement over the height corresponding to the temperature limits indicated. For the network model these are local values.

Thus it can be seen that the structure between lg $T = 5.5$ and 5.8 can be accounted for by the deposit of 4×10^6 erg $\mathrm{cm}^{-2}\,\mathrm{s}^{-1}$ of mechanical energy, mostly in the region lg $T = 5.6$. However, the region lg $T = 4.8$ to 5.5 can only be explained by the *emission* of energy, e.g. by the propagation of mechanical energy from this region to other parts of the atmosphere. This requirement has been noted by Kuperus & Athay (1967) who suggested that it may provide the energy source for spicule formation. It is difficult to find an adequate physical explanation of either the emission

PHILOSOPHICAL TRANSACTIONS OF THE ROYAL SOCIETY A MATHEMATICAL, PHYSICAL & ENGINEERING SCIENCES

or absorption of this mechanical energy over the very small distances that these temperature intervals correspond to in the steep transition region.

It is proposed here that the difficulty of reconciling the two approaches to the determination of atmospheric structure is due to the shortcomings of the spherical symmetry assumption. An inhomogeneous model of the atmosphere will be developed which, it will be shown, goes a long way to removing the discrepancy between the absolute intensity and energy balance analyses.

3. Network effects

3.1. *Observations*

In recent years it has become possible to record spatially resolved images of the solar disk in the ultraviolet with high spatial resolution. These include observations from rocket vehicles (Tousey 1971) and from the Apollo telescope mount on Skylab (Tousey *et al.* 1973, Reeves *et al.* 1974). The most striking feature of images formed in transition region lines is the strong intensity enhancement at the supergranule boundaries (s.g.b.) as compared with the central areas of the supergranule cells (s.g.c.) The preliminary analysis presented by Reeves *et al.* shows that this is true of a wide range of lines formed in the temperature range 10^4–3×10^5 K. Within experimental uncertainties, the appearance is similar for all of these lines; the width of the s.g.b. is of the order 10″ and the contrast between the s.g.b. and s.g.c. is about a factor of 10. In view of this high contrast factor it is clear that a spherically averaged model is a hazardous approximation. For lines formed in the range 10^4 K to 3×10^5 K it can be stated that approximately 85 % of the observed intensity originates from 35 % of the solar surface at the s.g.b. For lines formed at higher temperatures of 1.5×10^6 K the pattern has disappeared. The pattern can be shown to overlay precisely the Ca K network formed at a lower height, and the magnetic enhancement at the s.g.b. observed at photospheric levels. It is assumed that the intensity enhancement is associated with the magnetic flux concentrations. At photospheric levels the flux is driven to the s.g.b. by convective motions. At higher levels this flux expands until higher in the corona where the plasma pressure is smaller, it has become uniform.

3.2. *Network models*

There have been at least two previous attempts to construct a network model. The first by Kopp & Kuperus (1968) is based on the assumption that the flux concentration continues up to some arbitrary height in the chromosphere, and then expands with a potential field distribution. Their analysis is carried out for the two flux lines which remain vertical; one at the centre of the s.g.b. and one at the centre of the s.g.c. This leads to a serious error, because the centre of the s.g.c. is a singular point which is *not* typical of neighbouring areas. They predicted an enhanced emission at the s.g.c., an opposite situation to that observed, but did not have the advantage of any observations at that time to guide them.

A later analysis by Kopp (1972) was able to draw on some observations. Kopp dealt in detail with the s.g.b. and introduced an area factor for the flux concentration which increased with height. He was able to derive some useful results for the effects of the s.g.b. on energy balance. However, the situation at the s.g.c. was not analysed. The assumption made by Kopp that the field above the s.g.b. is approximately vertical will be seen later to be a poor approximation.

3.3. *Present approach*

In the present paper we attempt to derive a model of the network structure based upon a realistic theory for the field configuration as it expands with height. Since it is the supergranule convection cell which concentrates the flux at the photosphere, it must also be the vertical extent of this cell that determines the rate of expansion of the flux. This rate in turn determines the inclination and tapering of the flux tubes, which are all critical parameters in deriving an atmospheric structure. The analysis is based upon a two dimensional geometry, since the s.g.b. extends linearly in the third dimension. It is also assumed, as with other analyses, that the flux tubes are not twisted helically and that we are dealing with a cell within a large area on the Sun having a single magnetic polarity.

4. Magnetic field configuration

The model derived is shown in figure 5, which represents a vertical section through a supergranule cell. It is assumed that the magnetic flux is totally excluded from the cell so that there is an interface between plasma having a velocity field but no magnetic field, and plasma having a magnetic field but no velocity. This assumption is not a necessary one, but greatly simplifies the treatment. It is also proposed that it is a reasonable description of the situation. If instead we start with flux permeating the cell, it can be shown that the lifetime of a single cell (*ca.* 20 h) is insufficient to produce the observed flux concentration at the s.g.b. It is more likely that the flux having been concentrated outside the cell, it simply moves to the new cell boundaries as the network evolves, but remains concentrated. Alternatively, since it is believed that all the flux arises in the

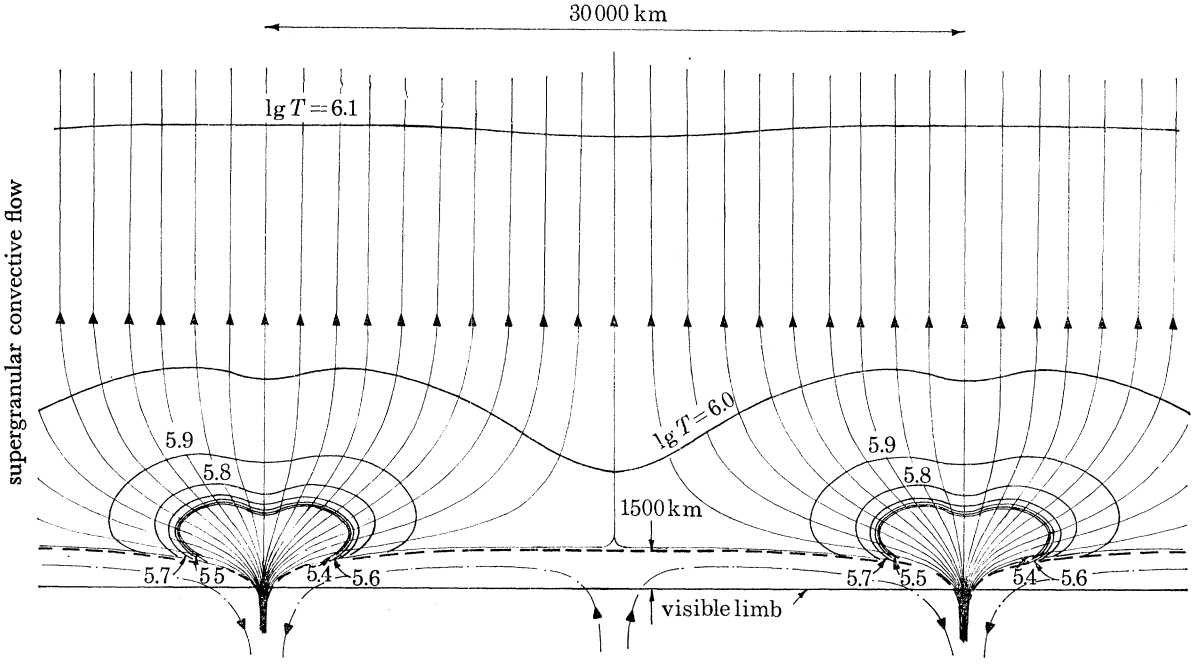

Figure 5. The proposed structure of the network model based upon energy balance (model C), showing the convection cell, magnetic field lines and contours of constant temperature. The primary transition region is indicated by the converging contours of temperature. The secondary transition region is shown by the dashed line.

first place from emerging loops, it is likely that these slip between the cells as they emerge, and never penetrate the convecting material.

It is now possible to write down the equation for pressure balance across the cell/boundary interface

$$N(C)\,kT = N(B)\,kT + B^2/8\pi, \tag{6}$$

which remains valid even allowing for field curvature, where $N(C)$ and $N(B)$ are the total number density of the cell and boundary respectively, and B is the magnetic field. Since $N(C)$ and $N(B)$ have approximately the same density scale height, $N(B)/N(C) = \alpha$ will be constant with height. Then

$$N(C)\,kT(1-\alpha) = B^2/8\pi. \tag{7}$$

$N(C)$ is assumed to have the usual chromospheric scale height, and α is given an assumed value of 0.9. If α were much closer to 1 it would not be possible to produce the observed flux compression, whereas if it were much smaller, e.g. 0.5, the density variations at photospheric level would be seen as a prominent 'photospheric network'. The precise value of α, while important for convection theory, is not critical in the present analysis, and the above treatment is quite adequate to give the correct geometric shape to the expanding flux.

The solution of equation (7), together with the requirement for conservation of flux, gives a first approximation for the boundary of the cell, shown as a dashed line in figure 5. This surface, which excludes the magnetic flux is treated as a perfectly conducting surface, having constant magnetic vector potential, and the field outside of it solved in $\boldsymbol{\nabla} \times \boldsymbol{B} = 0$ approximation. The cell boundary is then adjusted iteratively in order to continue satisfying equation (7). The value of B in the corona has been taken as 1 G† for the model in figure 5.

5. The magnetic model

We cannot directly construct a two-dimensional atmospheric model based upon observed intensities, since we do not have sufficient data to assign an emission measure to each of the flux tubes. We must therefore adopt an energy balance method to determine the atmosphere. It is now necessary to make some further assumptions. The first of these is that a quasi-steady-state solution is acceptable. In terms of the lifetime of the supergranule cells, this is amply justified. It is further assumed that the plasma has infinite conductivity, i.e. cannot cross magnetic field lines. The general hydrostatic equilibrium equation then becomes

$$\boldsymbol{\nabla} p = \frac{1}{4\pi}\boldsymbol{\nabla} \times \boldsymbol{B} \times \boldsymbol{B} - \rho \boldsymbol{\nabla} \phi, \tag{8}$$

where ϕ is the gravitational potential. We now assume that heat conduction is constrained to flow along the field lines, and construct an energy balance model satisfying equations (3) and (8). This can be accomplished by a process of iteration. For the first step it has already been assumed that $\boldsymbol{\nabla} \times \boldsymbol{B} = 0$ except at the interface with the cell, i.e. that there are no coronal currents, or that the plasma pressure does not distort the field lines. After computing the plasma distribution it is possible using equation (8) to compute $\boldsymbol{\nabla} \times \boldsymbol{B}$ and then to correct the field distribution for this effect. However, it is now clear that this will have a negligible effect on the geometric shape

† $1\ \mathrm{G} \equiv 10^{-4}\ \mathrm{T}$.

of the flux tubes, so that for the present purposes the iteration is unnecessary and $\nabla \times \boldsymbol{B} = 0$ will be assumed.

The problem now reduces to the simple one of establishing an energy balance atmosphere within each flux tube, treated as a rigid tube isolated from its neighbours. The boundary conditions adopted are based upon observations of coronal temperature and density and the observational result that, for ions formed at coronal temperatures, the supergranule network is not observed. Thus each flux tube has the same values for N_e and T at 30 000 km, the maximum height of the computation, and it is also implied that each tube has the same conductive flux F_c at this point. The value of F_c has been selected to give the best fit with observations, and in the case of figure 5 is 3.6×10^5 erg cm^{-2} s^{-1} at 30 000 km height. If the mechanical energy flux is also ducted along the field lines, then the entire flux heating the corona must originate from the turbulent motions at narrow regions along the supergranule boundaries. The resulting structure differs from the spherically symmetric structure now on account of two factors alone. These are the inclination and the tapering of the flux tubes. $\nabla \cdot \boldsymbol{F}_c$ must now take account of derivatives in two dimensions. Figure 5 shows the contours of constant T, which have been plotted as far down as lg T of 5.4, where they converge rapidly on the steep transition region. We will refer to this energy balance network model as shown in figure 5 as model C. It can be seen that the position of the transition region for flux tubes which in the corona are above the cell centres is such that when viewed normally, this region does not overlay the cell centres. It is limited to a strip at the s.g.b. which is 10″ in width, i.e. fully consistent with the ultraviolet observations.

We will refer to this steep transition region within the flux tubes as the 'primary transition region'. It is analogous to the transition region resulting from spherically symmetric analyses, the gradient being determined mainly by thermal conduction. As suggested by Kopp, since it covers only one third of the solar disk, in order to keep the same emission measure, it will have a gradient smaller by a factor 3 and total conducted flux smaller by 3^2 or *ca.* 10 than the spherically symmetric absolute intensity models; i.e. 3.6×10^5 erg cm^{-2} s^{-1} instead of *ca.* 3×10^6 erg cm^{-2} s^{-1}.

Outside of this s.g.b. 10″ region, there is an interface between the cell plasma at chromospheric temperatures and the overlying coronal plasma at *ca.* 10^6 K, which we will term the 'secondary transition region'. In the limited approximation made here, this region will be strictly parallel to the field; i.e. zero heat conduction across it, an infinite gradient, and thus no material at intermediate temperatures. This is clearly not so, since such a steep gradient would certainly give rise to local instabilities and mixing and thus to some plasma at transition temperatures. In fact we know from the observed intensities that the gradient here will be about 10 times steeper than the primary transition region, or about 3 times steeper than that predicted by spherically symmetric absolute intensity models.

The similarity in structure and contrast of the observed s.g.b. from the middle chromosphere through the transition region led Reeves *et al.* (1974) to suggest that the magnetic field pattern is essentially vertical up to 3×10^5 K and thereafter changes abruptly to a reduced vertical component by 1.5×10^6 K. It can be seen from figure 5 that this is not a necessary requirement from the observations; indeed the apparent abrupt change is due to the steepness of the transition region, and arises from the use of the temperature scale instead of a distance scale. Moreover, the model in figure 5 suggests that the edges of the s.g.b. are defined by field that is not vertical but nearly horizontal.

PHILOSOPHICAL TRANSACTIONS OF THE ROYAL SOCIETY A MATHEMATICAL, PHYSICAL & ENGINEERING SCIENCES

6. Predictions from the magnetic model

6.1. *Temperature against height*

With a two-dimensional model it is of course not possible to use a single curve to display T against h. However, since we know that observations of the transition region are strongly weighted to the s.g.b., there is some value in comparing the structure above the centre of the s.g.b. with that obtained from the absolute intensities. This has been done in figure 2 where the network has the effect of bringing the T against h curve much closer to the spherically symmetric absolute intensity model. Compared with the spherical energy balance models, the effect of the network is to increase the gradient at lower temperatures, thereby lowering the level at which a temperature of 10^6 K occurs. This is a direct result of the tapering of the magnetic field lines.

6.2. *Emission measure*

A more satisfactory way of comparing the predictions with observations is to compare the computed and observed emission measure $\langle N_e^2 \mathrm{d}h/\mathrm{d}\lg T\rangle$; or rather $\langle N_e^2 \mathrm{d}V/\mathrm{d}\lg T\rangle$ per unit area, since T is not only a function of height. The computed emission measure has been added as model C to the curves in figure 3. It is seen at once that over the range of lg T from 5.2 to 6.2 it now agrees well with the observed intensities, both in slope and in absolute magnitude. In view of the large discrepancy on this plot for spherical energy balance models, this is regarded as strong evidence for the validity of the network configuration derived. However, for temperatures below lg T of 5.2 this model still diverges from the observed intensities. The reasons for this are discussed below in § 7.

6.3. *Limb observations*

It is obvious that the height distribution of transition region material shown in figure 5 must have important consequences for observations made at the limb. It should first be noted that the above model takes no account of spicules, which presumably represent further extensions of chromospheric material above the s.g.b. regions. However, the work of Burton, Jordan, Ridgeley & Wilson (1973) indicated that the contributions from spicules to transition region radiation is very small.

Observations of transition region lines at the limb have been made from a rocket during the 7 March 1970 total solar eclipse (Gabriel *et al.* 1971). The data includes observations during second contact when the moon is progressively obscuring layers up to increasing heights in the solar atmosphere. Figure 6 shows the result of a preliminary analysis of this data for a quiet region at the limb (Gabriel & C. Jordan, unpublished material). A more complete analysis is at present in progress. From figure 6 it can be seen that the transition region lines of Fe II, Si III, He II and O VI fall to say one third of their integrated intensity above the limb when the emission is obscured below 3000 km. Since the geometry of the experiment is well known, these heights are on an absolute scale. This progressive obscuration is consistent with the model shown in figure 5, but is not at all what one would expect from a spherically symmetric model.

Observations of the Sun at millimetre wavelengths show continuum emission which reaches unit optical depth at regions in the chromosphere. For a spherically symmetric atmosphere a characteristic limb brightening would be expected. In practice, limb darkening is observed for $\lambda = 3.5$ mm and below. Lantos & Kundu (1972) have attempted to analyse observations of limb effects made at 1.2 mm, 3.5 mm and 9 mm wavelengths on the basis of inhomogeneities. This analysis requires an approach in which various models are evaluated to see how well they predict

PHILOSOPHICAL TRANSACTIONS OF THE ROYAL SOCIETY A MATHEMATICAL, PHYSICAL & ENGINEERING SCIENCES

the observations. Various spicule models were examined for fit. The spicule model of Beckers (1968) was found adequate above 3000 km. However, it required an empirical adjustment so that below 2000 km the area covered by spicules was increased from 3 to 40 %. This is precisely what one would expect if one includes in addition to spicules, the ridges of chromosphere covering the s.g.b. as shown in figure 5.

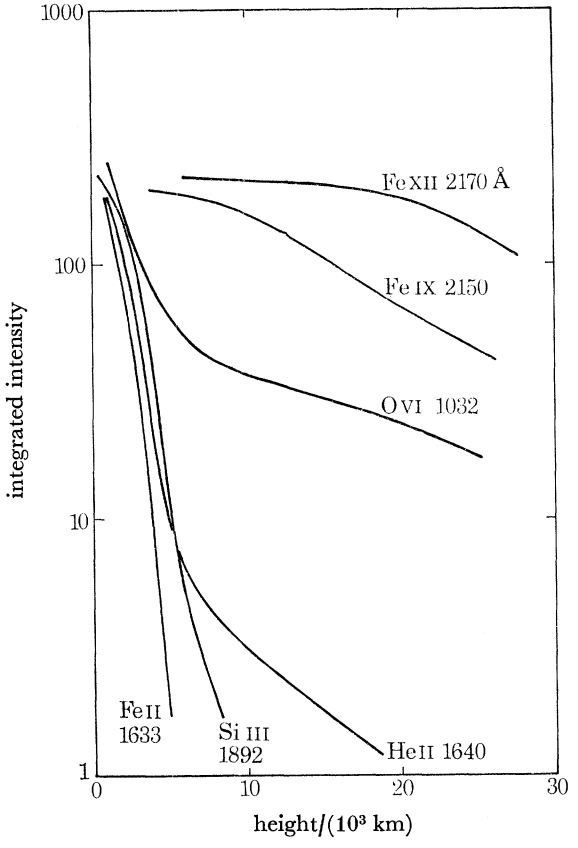

FIGURE 6. Preliminary analysis of 1970 eclipse data showing the integrated intensity in various spectral lines above a height h, as a function of h for a quiet region on the solar limb.

6.4. *Intensity distribution*

From model C in figure 5 it is possible to compute the detailed intensity distribution across a s.g.b. in a spectral line formed in the transition region. This distribution is shown in figure 7, for an optically thin emission line. The steep enhancement at the edges of the s.g.b. region is in effect a 'limb brightening' process at the edges of the ridge overlaying the s.g.b. The present observations from Skylab are limited in spatial resolution to *ca.* 5″ or a little better. They would therefore be insufficient to observe this effect. New observations from OSO-I may however reach a spatial resolution of 1″, so that this limb brightening might be seen. However, the effect predicted in figure 7 is somewhat dependent on the idealized aspects of the assumptions. It is known that in practice the s.g.b. is not a parallel, cleanly bounded region of uniform magnetic field, but is spatially deformed with large variations in the local photospheric field values. Whereas this deformation is expected to have very little effect on the model shown in figure 5, it may completely obscure the narrow brightening regions predicted in figure 7.

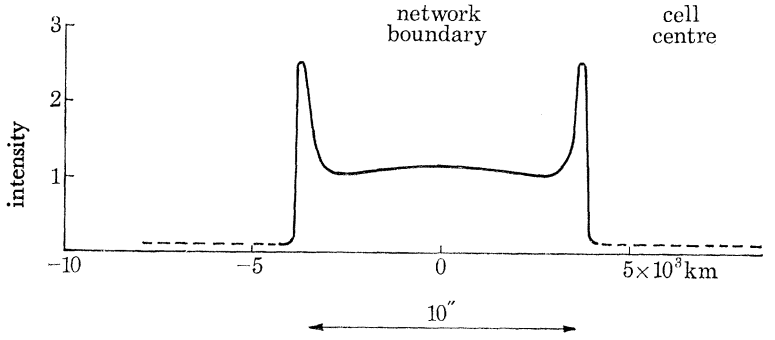

FIGURE 7. Predicted intensity trace across a supergranule boundary for a transition region line.

6.5. *Density distribution*

In the earlier work (Gabriel 1974) it was predicted that the electron density at a given temperature at the s.g.b. would be lower than that observed at the s.g.c. While this prediction is still valid, the magnitude of the effect is now thought to be very small (much less than a factor of 2), and may well not be measurable. Nevertheless, measurements of this effect would be important in establishing the validity of the model.

7. ABSOLUTE INTENSITIES NETWORK MODEL

As indicated above, the lack of appropriate observations precludes the determination of a complete network model based upon observed intensities. However, the agreement above $\lg T = 5.2$ between model C and the integrated observed intensities (see figure 3) leads to the possibility of determining an approximate structure, valid directly above the s.g.b. The method is as follows. From model C in figure 5 (network with energy balance) an area factor $a(T)$ is determined as a function of T for the centre-line of the s.g.b. for $\lg T > 5.2$. This factor $a(T)$, which is unity higher in the corona has fallen to 0.32 at $\lg T = 5.2$, and is then assumed to remain constant at this figure for lower temperatures. This is physically justified by the very small thickness of the transition region. The observed emission measure is assumed to originate entirely from the s.g.b. in such a way that the local value at the centre of the s.g.b. is obtained by dividing the mean value by $a(T)$. The resulting modified emission measure can be integrated together with equation (2) to give a structure which we will designate model D. This model has been detailed in table 1. As expected, it is very close to the centre-line values of model C above $\lg T \approx 5$ but deviates significantly at lower T. This deviation is best understood by deriving the effective mechanical energy deposition S. S has been plotted in figure 4, where it has been compared with the spherical absolute intensity model A. The energy balance model C would of course give $S = 0$ throughout. It would appear from figure 4, that the discrepancy below $\lg T = 5.2$ for model C is due to the failure to take account of an energy deposition amounting to 2×10^6 erg cm^{-2} s^{-1} locally (or mean value of 6×10^5 erg cm^{-2} s^{-1}) between $\lg T = 4.3$ and 5.0.

Compared with model A, the embarrassing negative value of S between $\lg T = 5$ and 5.5 now drops from 1.7 to 0.08 erg cm^{-3} s^{-1}. Integrated over height, this drop is from 3×10^6 erg cm^{-2} s^{-1} to 7×10^5 erg cm^{-2} s^{-1} locally or mean value of 2×10^5 erg cm^{-2} s^{-1}. The errors in this type of analysis are large since S is the difference between two large quantities $-\boldsymbol{\nabla} \cdot \boldsymbol{F}_c$ and R, and $-\boldsymbol{\nabla} \cdot \boldsymbol{F}_c$ depends on the second derivative of T with respect to height. The figure of 2×10^5 erg cm^{-2} s^{-1} is therefore close to the error limit and the negative value of S can now be discounted as

a problem. Note also that the positive value of S required by the spherical model A between lg T of 5.5 and 5.7 has now vanished for the network model D.

8. Other effects

It is worth recalling two assumptions which have been made in the present analysis, the validity of which cannot be proven. The first, implicit in the analysis of absolute intensities, is the assumption that the relative element abundances remain constant. Various workers (e.g. Delache 1967) have shown that thermal diffusion can result in variations in heavy element abundances in the steep transition region. No observational evidence for this has been found, and it has been argued that turbulent velocities (which are observed) will act so as to cancel this effect.

The second assumption is the neglect from the hydrostatic equilibrium equation (2) of terms due to mechanical wave motions. Delache (1967) and McWhirter *et al.* (1975) have both discussed this effect. Loulergue & Nussbaumer (1974) have suggested that this term acts so as to decrease the gas pressure in the transition region, increasing its thickness by factors of about 10 to 20. The evaluation of such terms is very difficult. The additional pressure terms depend upon details of the diffraction and absorption of wave motions which are not well understood. It must be admitted that such collective pressure terms may have a significant effect, particularly on the type of analysis shown in figure 4. However, it would seem that we can discount any large increase in the thickness of the transition region. Model D predicts a thickness of 400 km for the temperature interval lg T 4.3 to 5.5. Existing observations (Burton *et al.* 1973) would be inconsistent with any large increase in this figure.

9. Conclusions

It has been shown that when carrying out analyses in a spherically symmetric geometry, there are important discrepancies between the solar atmosphere models derived from absolute spectral intensities (model A) and energy balance considerations (model B). In an attempt to reconcile these, a two dimensional inhomogeneous model has been derived based upon the effects of supergranule convection. The shape of the expanding magnetic flux is determined by the vertical extent of the convection cells. A two-dimensional atmospheric model based upon energy balance (model C) is found to agree well with the mean observed emission measure above lg $T = 5.2$, as well as with several other observational data. Below lg $T = 5.2$ mechanical energy deposition becomes important and it is better to use a modified model (model D) based upon observed absolute intensities. Model D is available only in one-dimensional form for use directly above the supergranule boundary, where it agrees closely with model C for lg $T > 5.2$. The models presented all neglect the contribution of non-thermal pressure terms, but it is expected that these will not be very important at temperatures above lg $T = 4.3$.

I should like to thank Miss K. Dickson for her assistance with the programming and computing aspects of this work. This paper is published with the permission of the Director of the Appleton Laboratory.

PHILOSOPHICAL TRANSACTIONS OF THE ROYAL SOCIETY A MATHEMATICAL, PHYSICAL & ENGINEERING SCIENCES

References (Gabriel)

Athay, R. G. 1966 *Astrophys. J.* **145**, 784.

Beckers, J. M. 1968 *Solar Phys.* **3**, 367.

Burton, W. M., Jordan, C., Ridgeley, A. & Wilson, R. 1973 *Astron. Astrophys.* **27**, 101.

Delache, P. 1967 *Ann. d'Astrophys.* **30**, 827.

Dupree, A. K. & Goldberg, L. 1967 *Solar Phys.* **1**, 229.

Dupree, A. K., Huber, M. C. E., Noyes, R. W., Parkinson, W. H., Reeves, E. M. & Withbroe, G. L. 1973 *Astrophys. J.* **182**, 321.

Gabriel, A. H. 1974 In *Chromopheric fine structure* (ed. R. G. Athay). Proc. I.A.U. Symp. No. 56. Holland: Reidel.

Gabriel, A. H., Garton, W. R. S., Goldberg, L., Jones, T. J. L., Jordan, C., Morgan, F. J., Nicholls, R. W., Parkinson, W. H., Paxton, H. J. B., Reeves, E. M., Shenton, D. B., Speer, R. J. & Wilson, R. 1971 *Astrophys. J.* **169**, 595

Jordan, C. 1965 Ph.D. Thesis, University of London.

Jordan, C. & Wilson, R. 1971 In *Physics of the solar corona* (ed. Macris). Holland: Reidel.

Kopp, R. A. 1972 *Solar Phys.* **27**, 373.

Kopp, R. A. & Kuperus, M. 1968 *Solar Phys.* **4**, 212.

Kuperus, M. & Athay, R. A. 1967 *Solar Phys.* **1**, 361.

Lantos, P. & Kundu, M. R. 1972 *Astron. Astrophys.* **21**, 119.

Loulergue, M. & Nussbaumer, H. 1974 *Astron. Astrophys.* **34**, 225.

Malinovsky, M. & Heroux, L. 1973 *Astrophys. J.* **181**, 1009.

McWhirter, R. W. P., Thoneman, P. C. & Wilson, R. 1975 *Astron. Astrophys.* **40**, 63. (See also McWhirter, R. W. P. & Wilson, R.; this volume.)

Reeves, E. M., Foukal, P. V., Huber, M. C. E., Noyes, R. W., Schmahl, E. J., Timothy, J. G., Vernazza, J. E. & Withbroe, G. L. 1974 *Astrophys. J.* **188**, L 27.

Tousey, R. 1971 *Phil. Trans. R. Soc. Lond.* A **270**, 59.

Tousey, R., Bartoe, J. D., Bohlin, J. D., Brueckner, G. E., Purcell, J. D., Scherrer, V. E., Sheeley, N. R., Schumacher, R. J. & Vanhoosier, M. E. 1973 *Solar Phys.* **33**, 265.

PHILOSOPHICAL TRANSACTIONS OF THE ROYAL SOCIETY A MATHEMATICAL, PHYSICAL & ENGINEERING SCIENCES